International Journal of Microwave and Wireless Technologies, 2013, 5(5), 611–619.
doi:10.1017/S1759078713000512

RESEARCH PAPER

Theoretical investigation of an air gap tuned superconducting triangular microstrip antenna

OUARDA BARKAT

An analytical model is presented to improve the performance of the equilateral triangular microstrip antenna (ETMA). An improved model is presented taking into account the insertion of an air gap between the substrate and the ground plane, and High T_c superconducting material (HTS) for the triangular patch. The full-wave spectral domain technique in conjunction with the complex resistive boundary condition is used to calculate the characteristics including resonant frequencies, bandwidths, and radiation efficiency. Numerical results for the air gap tuning effect on the operating frequency and bandwidth of the high T_c superconducting triangular microstrip antenna (HTSTMA) are presented. The effect of temperature on resonant frequency and bandwidth of the HTSTMA are also given. The computed data are found to be in good agreement with results obtained using other methods.

Keywords: Equilateral triangular, Microstrip antenna, High T_c superconducting, Spectral method

Received 1 January 2013; Revised 24 April 2013; first published online 3 June 2013

I. INTRODUCTION

With the recent advances in wireless communication industry, there is an increasing demand for smaller antennas that can be easily integrated in monolithic microwave integrated circuits [1]. Among various types of planar antennas, the microstrip antenna provides all of the advantages of printed circuit technology. This antenna consists of a radiating patch on one side of a dielectric substrate; the patch is generally made of conducting material such as copper or gold and can take any possible shape. They have some drawbacks such as low radiation efficiency [2]. High T_c superconducting materials (HTS's) provide flexibility and accuracy in integrated circuit design, and can be used to overcome radiation efficiency of antennas [3–6]. The triangular microstrip antenna (TMA) is one of the most preferable for small equipment; it has the advantage of occupying less metalized area on the substrate than other existing configurations [7–15]. However, this will produce even lower gain and smaller bandwidth. An equilateral triangular microstrip antenna (ETMA) has a larger bandwidth compared to other triangular antenna.

Many techniques of bandwidth enhancement have been suggested and designed. Bandwidth of antenna can be increased by using the thick substrate of low dielectric constant or by designing the antenna in a multilayered media [9–11]. By introducing the air gap, we can obtain the tunable resonant frequency characteristics; it is possible to increase the bandwidth. The air gap idea, that an air gap between the substrate and the ground plane has been proposed by Lee and Dahele [7]. Recently, there have been a number of investigations of resonant frequencies of tunable equilateral triangular microstrip patch antennas. These investigations are based on the transmission-line model and the cavity model in simple computer aided design formulas for determining the tunable frequencies [9, 15]. However, the accuracy of these approximate models is limited and only suitable for analyzing simple, regularly shaped antenna or thin substrates. The full-wave spectral domain technique is extensively used in microstrip analysis and design [12, 16, 17]. This method gives better results than approximate techniques. In the current paper, we have developed an analytical model for analysis of high T_c superconducting triangular microstrip antenna (HTSTMA) with two lower substrates of which little has been published. Our theoretical study is carried out by using a full-wave spectral domain technique in conjunction with the complex resistive boundary condition.

Electronics Department, University of Constantine 1, 25000 Constantine, Algeria
Corresponding author:
O. Barkat
Email: barkatwarda@yahoo.fr

II. THEORETICAL MODEL

A) Geometrical structure

The air gap tuned HTSTMAs considered in this work are shown in Fig. 1. It was obtained by depositing a high T_c superconducting patch on a dielectric layer, which is mounted on air layer. This last layer is printed on the grounded plane. The upper layer being the dielectric substrate material is taken to be isotropic, has a uniform thickness of d_2. The

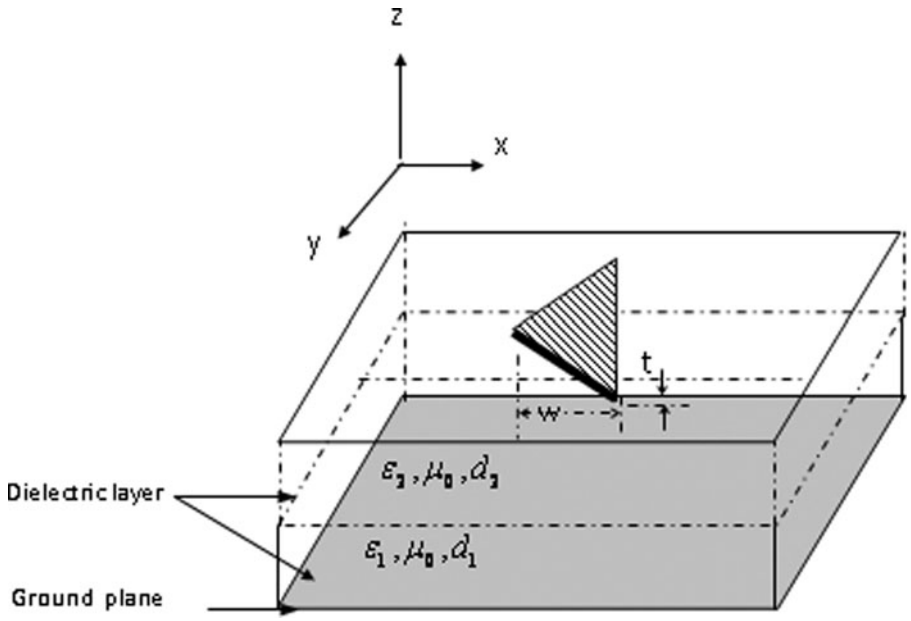

Fig. 1. Geometry of air gap tuned HTSTMA.

lower layer being the air gap of thickness d_1 has relative permittivity equal to 1. The high T_c superconducting triangular patch has thickness t, and side length W.

B) Theory

In this subsection, the full-wave spectral domain approach is used for analysis and design of an air gap tuned HTSTMAs. In this approach, starting from Maxwell's equations in the spectral domain, the general equations of the electric and magnetic transverse fields inside the j layer can be written as [18]

$$\bar{E}(r_s, z) = \begin{bmatrix} E_x(r_s, z) \\ E_y(r_s, z) \end{bmatrix} = \frac{1}{4\pi^2}\int_{-\infty}^{+\infty}\int_{-\infty}^{+\infty} \bar{F}(k_s, r_s)\,\tilde{\bar{e}}(k_s, z)dk_x\,dk_y, \tag{1}$$

$$\bar{H}(r_s, z) = \begin{bmatrix} H_y(r_s, z) \\ -E_x(r_s, z) \end{bmatrix} = \frac{1}{4\pi^2}\int_{-\infty}^{+\infty}\int_{-\infty}^{+\infty} \bar{F}(k_s, r_s)\,\tilde{\bar{h}}(k_s, z)dk_x\,dk_y, \tag{2}$$

Where

$$\bar{F}(k_s, r_s) = \frac{1}{k_s}\begin{bmatrix} k_x & k_y \\ k_y & -k_x \end{bmatrix} e^{ik_s \cdot r_s}, \tag{3}$$

With

$$k_s = k_x\,\hat{x} + k_y\,\hat{y}, \quad r_s = x\,\hat{x} + y\,\hat{y},$$

The superscripts of e and h in (1) and (2) denote the TM and TE waves, which are defined as

$$\tilde{\bar{e}}(k_s, z) = \bar{A}_j e^{-ik_{zj}z} + \bar{B}_j e^{ik_{zj}z}, \tag{4}$$

$$\tilde{\bar{h}}(k_s, z) = (\bar{A}_j e^{-ik_{zj}z} - \bar{B}_j e^{ik_{zj}z}) \cdot \bar{g}_j(k_s), \tag{5}$$

with

$$\bar{g}_j = \begin{vmatrix} \dfrac{\omega\varepsilon_0\varepsilon_j}{k_{zj}} & 0 \\ 0 & \dfrac{k_{zj}}{\omega\mu_0} \end{vmatrix}, \tag{6}$$

where A_j and B_j are unknown vectors.

Writing (4) and (5) at the interfaces of the layer (Fig. 2), and by eliminating the unknowns A_j and B_j, we obtain the matrix form

$$\begin{bmatrix} \tilde{\bar{e}}\left(k_s, z_j^-\right) \\ \tilde{\bar{h}}\left(k_s, z_j^-\right) \end{bmatrix} = \bar{T}_j \begin{bmatrix} \tilde{\bar{e}}\left(k_s, z_{j-1}^+\right) \\ \tilde{\bar{h}}\left(k_s, z_{j-1}^+\right) \end{bmatrix}, \tag{7}$$

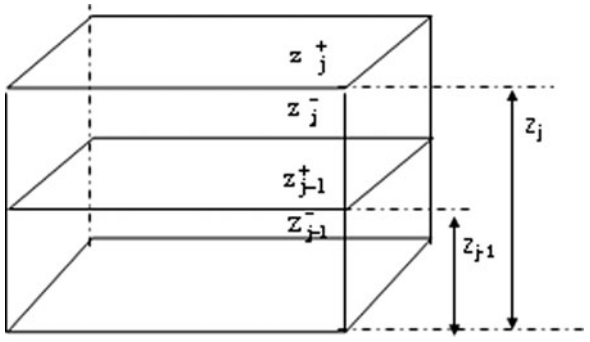

Fig. 2. Geometry of layers.

https://doi.org/10.1017/S1759078713000512 Published online by Cambridge University Press

With

$$\bar{T}_j = \begin{bmatrix} \bar{I}\cos(\bar{k}_{zj}d_j) & -i\bar{g}_j^{-1}(k_s)\sin(\bar{k}_{zj}d_j) \\ -i\bar{g}_j(k_s)\sin(\bar{k}_{zj}d_j) & \bar{I}\cos(\bar{k}_{zj}d_j) \end{bmatrix}, \quad (8)$$

Where $\bar{I}$ being the (2 × 2) unit matrix and $\bar{k}_{zj}$ is given by

$$\bar{k}_{zj} = \begin{vmatrix} k_{zj} & 0 \\ 0 & k_{zj} \end{vmatrix}. \quad (9)$$

The relation between the tangential electric and magnetic field components in dielectric layers below the patch interface is given by

$$\begin{bmatrix} \tilde{\bar{e}}(k_s, z_M^-) \\ \tilde{\bar{h}}(k_s, z_M^-) \end{bmatrix} = \bar{T}_1\ \bar{T}_2\ \bar{T}_3 \ldots \bar{T}_M \begin{bmatrix} \tilde{\bar{e}}(k_s, 0) \\ \tilde{\bar{h}}(k_s, 0) \end{bmatrix}. \quad (10)$$

Above the patch interface, the relation between the tangential electric and magnetic field components in dielectric layers is given by

$$\begin{bmatrix} \tilde{\bar{e}}(k_s, z_N^+) \\ \tilde{\bar{h}}(k_s, z_N^+) \end{bmatrix} = \bar{T}_{M+1}\,\bar{T}_{M+2}\,\bar{T}_{M+3} \ldots \bar{T}_N \begin{bmatrix} \tilde{\bar{e}}(k_s, z_M^+) \\ \tilde{\bar{h}}(k_s, z_M^+) \end{bmatrix}. \quad (11)$$

We can put the product matrix as

$$\bar{\Gamma}_< = \prod_{j=M}^{1} \bar{T}_j = \begin{bmatrix} \Gamma_<^{11} & \Gamma_<^{12} \\ \Gamma_<^{21} & \Gamma_<^{22} \end{bmatrix} \quad (12)$$

and

$$\bar{\Gamma}_> = \prod_{j=N}^{M+1} \bar{T}_j = \begin{bmatrix} \Gamma_>^{11} & \Gamma_>^{12} \\ \Gamma_>^{21} & \Gamma_>^{22} \end{bmatrix}, \quad (13)$$

where $\prod_{j=M}^{1}$ and $\prod_{j=N}^{M+1}$ means the product of matrices above and below the patch.

By using the continuity equations for the tangential field components, we have

$$\tilde{\bar{e}}\left(k_s, z_j^+\right) = \tilde{\bar{e}}\left(k_s, z_j^-\right), \quad (14)$$

$$\tilde{\bar{h}}(k_s, z_p^+) = \tilde{\bar{h}}(k_s, z_M^-) + \tilde{\bar{J}}(k_s),\ j = 1, N. \quad (15)$$

The electric field boundary condition at $z = 0$ will lead to

$$\tilde{\bar{e}}(k_s, 0) = \bar{0}. \quad (16)$$

Finally, the radiation condition in the air region above the top layer of the structure yields, is given by

$$\tilde{\bar{e}}(k_s, z_N^+) = \bar{g}_0\,\tilde{\bar{h}}(k_s, z_N^+), \quad (17)$$

where $\bar{g}_0$ can be obtained from the expression of $\bar{g}_j$ given in (6) by allowing $\varepsilon_j = 1$

Combining (10)–(17), we find that the relationship between the patch current and the electric field on the patch is given by

$$\tilde{\bar{E}}(\boldsymbol{k}_s) = \bar{\boldsymbol{G}}(\boldsymbol{k}_s)\,\tilde{\bar{J}}(\boldsymbol{k}_s), \quad (18)$$

where $\tilde{\boldsymbol{J}}(\boldsymbol{k}_s)$ is the current on the patch, and $\bar{\boldsymbol{G}}$ is the spectral dyadic Green's function, its expression is shown to be given by [19]

$$\bar{G}(k_s) = \begin{bmatrix} G_{xx} & G_{xy} \\ G_{yx} & G_{yy} \end{bmatrix} = \frac{1}{k_s^2} \begin{bmatrix} k_x & k_y \\ k_y & -k_x \end{bmatrix} \bar{Q} \begin{bmatrix} k_x & k_y \\ k_y & -k_x \end{bmatrix}, \quad (19)$$

where Q is given by

$$\bar{Q}(k_s) = -\left(\bar{\Gamma}_<\right)_{12}\left[\bar{g}_0\left(\bar{\Gamma}_>\right)_{12} - \left(\bar{\Gamma}_>\right)_{22}\right]\left[\bar{g}_0\left(\bar{\Gamma}\right)_{12} - \left(\bar{\Gamma}\right)_{22}\right]^{-1}. \quad (20)$$

After some algebraic operations, Q is given by

$$\bar{Q}(\boldsymbol{k}_s) = \begin{vmatrix} \frac{D_e}{T_e} & 0 \\ 0 & \frac{D_h}{T_h} \end{vmatrix}, \quad (21)$$

in which

$$D_e = -ik_0^2[\sin(k_{z1}d_1)\cos(k_{z2}d_2) + \frac{k_{z1}}{k_{z2}}\cos(k_{z1}d_1)\sin(k_{z2}d_2)],$$

$$T_e = \omega\varepsilon_0\Big[\cos(k_{z2}d_2)\,[k_{z1}\cos(k_{z1}d_1) + ik_{z0}\sin(k_{z1}d_1)] + i\sin(k_{z2}d_2)\Big[\frac{k_{z0}k_{z1}}{k_{z2}}\cos(k_{z1}d_1) + ik_{z2}\sin(k_{z1}d_1)\Big]\Big],$$

$$D_h = -i[k_{z0}k_{z1}\sin(k_{z1}d_1)\cos(k_{z2}d_2) + \frac{\varepsilon_{r1}}{\varepsilon_{r2}}k_{z0}k_{z2}\cos(k_{z1}d_1) \times \sin(k_{z2}d_2)],$$

$$T_h = \omega\varepsilon_0[\cos(k_{z2}d_2)\,[\varepsilon_{r1}k_{z0}\cos(k_{z1}d_1) + ik_{z1}\sin(k_{z1}d_1)] + \sin(k_{z2}d_2)\Big[\frac{\varepsilon_{r1}}{\varepsilon_{r2}}k_{z2}\cos(k_{z1}d_1) + i\varepsilon_{r2}\frac{k_{z0}k_{z1}}{k_{z2}}\sin(k_{z1}d_1)\Big]\Big],$$

where

$$k_s = \left(k_x^2 + k_y^2\right)^{1/2}, \quad k_{z0} = \left(k_0^2 - k_s^2\right)^{1/2}, \quad k_0 = \left(\omega^2\varepsilon_0\mu_0\right)^{1/2},$$

$$k_{z1} = \left(k_1^2 - k_s^2\right)^{1/2}, \quad k_1 = \left(\omega^2\varepsilon_0\varepsilon_{r1}\mu_0\right)^{1/2},$$

$$k_{z2} = \left(k_2^2 - k_s^2\right)^{1/2}, \quad k_2 = \left(\omega^2\varepsilon_0\varepsilon_{r2}\mu_0\right)^{1/2}.$$

https://doi.org/10.1017/S1759078713000512 Published online by Cambridge University Press

Integral equation method in conjunction with the Galerkin method has been a very popular choice for electromagnetic modeling. It gives the fundamental quantity of interest, namely electric current distribution on the patch surface from, which all the other required antenna parameters can be obtained. From this analysis, the surface current on the patch can be expanded into a series of known basis functions J_{xn} and J_{ym}

$$\bar{\boldsymbol{J}}(\boldsymbol{r}_s) = \sum_{n=1}^{N} a_n \begin{bmatrix} J_{xn}(\boldsymbol{r}_s) \\ 0 \end{bmatrix} + \sum_{m=1}^{M} b_m \begin{bmatrix} 0 \\ J_{ym}(\boldsymbol{r}_s) \end{bmatrix}, \quad (22)$$

where a_n and b_m are the coefficients of the basis functions.

Unlike the rectangular, circular, and annular patches, the triangular patch does not have a simple current distribution. The choice of basis function (J_x, J_y) is very important for rapid convergence to true values. The following expressions give the current basis J_x and J_y when the x component is an even function of y, for the dominant mode TM_{10} [11]

$$J_x(x, y) = \cos\left(\frac{2\pi y}{3W}\right) \cos\left(\frac{2\pi x}{W\sqrt{3}}\right), \quad (23)$$

$$J_y(x, y) = \sin\left(\frac{4\pi y}{3W}\right) - \sin\left(\frac{2\pi y}{3W}\right) \sin\left(\frac{2\pi x}{W\sqrt{3}}\right). \quad (24)$$

The Fourier transform of the basis function is obtained by using

$$\tilde{\bar{J}}(k_x, k_Y) = \frac{1}{\lambda_0^2} \int_0^W \int_{-x.tg(\pi/6)}^{x.tg(\pi/6)} \bar{J}(x, y) e^{i(k_x x + k_Y y)} dy dx. \quad (25)$$

To include the effect of the superconductivity of microstrip antenna in full-wave analysis, the impedance is determined by using London's equation and the model of Gorter and Gasimir, it is given by [20]

$$Z_S = R_S + iX_S, \quad (26)$$

where R_s and X_s are the surface resistance and surface reactance.

When the thickness t of the superconducting patch is less than three times the penetration depth λ_0 at zero temperature, the surface impedance can be approximated as follows:

$$Z_S = \frac{1}{t\sigma}. \quad (27)$$

The conductivity σ components are given by [21, 22].

$$\sigma = (\sigma_n (T/T_c)^4) - i\left(\frac{1 - (T/T_c)^4}{\omega \mu_0 \lambda_0^2}\right), \quad (28)$$

where σ_n is often associated with normal state conductivity at transition temperature of superconductor T_c and ω is the angular frequency.

The electric field integral equation which enforces the boundary condition must vanish on the patch surface,which is given by

$$\bar{\boldsymbol{E}}(\boldsymbol{r}_s) = \frac{1}{(2\pi)^2} \int d\boldsymbol{k}_s \, \boldsymbol{F}(\boldsymbol{k}_s, \boldsymbol{r}_s) \, (\bar{\boldsymbol{G}}(\boldsymbol{k}_s) - \overline{Z}_S) \, \tilde{\boldsymbol{J}}(\boldsymbol{k}_s) = 0, \quad (29)$$

where

$$\bar{Z}_S = \begin{vmatrix} Z_s & 0 \\ 0 & Z_s \end{vmatrix}.$$

Substituting (20) into (29) and using the selected basis functions as testing functions, we obtain the following homogeneous matrix equation:

$$\begin{bmatrix} [\bar{B}_{kn}]_{NxN} & [\bar{B}_{km}]_{NxM} \\ [\bar{B}_{\ln}]_{MxN} & [\bar{B}_{lm}]_{MxM} \end{bmatrix} \begin{bmatrix} [a_n]_{NX1} \\ [b_m]_{MX1} \end{bmatrix} = \begin{vmatrix} [0]_{NX1} \\ [0]_{MX1} \end{vmatrix}, \quad (30)$$

where

$$\bar{B}_{kn} = \int_{-\infty}^{+\infty} \int_{-\infty}^{+\infty} dk_s \frac{1}{k_s^2} (G_{xx} - Z_S) \tilde{J}_{xk}(-k_s) \tilde{J}_{xn}(k_s), \quad (31)$$

$$\bar{B}_{km} = \int_{-\infty}^{+\infty} \int_{-\infty}^{+\infty} dk_s \frac{k_x k_y}{k_s^2} G_{xy} \tilde{J}_{xk}(-k_s) \tilde{J}_{ym}(k_s), \quad (32)$$

$$\bar{B}_{\ln} = \int_{-\infty}^{+\infty} \int_{-\infty}^{+\infty} dk_s \frac{k_x k_y}{k_s^2} G_{yx} \tilde{J}_{yl}(-k_s) \tilde{J}_{xn}(k_s), \quad (33)$$

$$\bar{B}_{lm} = \int_{-\infty}^{+\infty} \int_{-\infty}^{+\infty} dk_s \frac{1}{k_s^2} (G_{yy} - Z_S) \tilde{J}_{yl}(-k_s) \tilde{J}_{ym}(k_s). \quad (34)$$

Therefore, for existence of nontrivial solutions, the determinant of (30) must be zero.

$$\det(\bar{B}(f)) = 0. \quad (35)$$

In general, the root of equation (35) is the complex resonant frequency ($f = f_r + if_i$), f_r is the resonant frequency, and $2f_i / f_r$ is the bandwidth of the antenna.

Once the complex resonant frequency is determined, the eigenvector corresponding to the minimal eigenvalue of the impedance matrix $\bar{B}$ gives the coefficients of the current on the triangular patch. Current density is thus obtained in the numerical form. This current density can be used for computing the radiation electric field from the vector Fourier transforms in the region $z \geq d_1 + d_2$ of Fig. 1.

$$\bar{E}(x, y, z) = \frac{1}{4.\pi^2} \int_{-\infty}^{+\infty} \int_{-\infty}^{+\infty} \tilde{\bar{E}}(k_x, k_x, d_1 + d_2) \times e^{-jk_0(z - d_1 - d_2).\cos(\theta)} e^{j(k_x.x + k_y.y)} dk_x dk_y. \quad (36)$$

Using the stationary phase method, we can obtain the far-zone field radiations.

https://doi.org/10.1017/S1759078713000512 Published online by Cambridge University Press

$$E_\varphi = jk_0 \frac{e^{-jk_0 r}}{2\pi r} e^{jk_0 \cos(\theta)(d_1+d_2)}(-\tilde{E}_x(k_x, k_y, d_1+d_2) \times \cos\varphi + \tilde{E}_y(k_x, k_y, d_1+d_2)\cos\varphi), \quad (37)$$

$$E_\theta = jk_0 \frac{e^{-jk_0 r}}{2\pi r} e^{jk_0 \cos(\theta)(d_1+d_2)}(\tilde{E}_x(k_x, k_y, d_1+d_2) \cos\varphi + \tilde{E}_y(k_x, k_y, d_1+d_2)\cos\varphi), \quad (38)$$

In equations (37) and (38), k_x and k_y are evaluated at the stationary phase point as

$$k_x = -k_0 \sin\theta \cos\varphi,$$

$$k_y = -k_0 \sin\theta \sin\varphi.$$

The benefits of using high temperature superconductors in microstrip antennas can be quite substantial owing to reduced losses, which translates to an increase in the efficiency of the antenna. The efficiency of the antenna can be defined as

$$\text{efficiency} = P_r/(P_r + P_c + P_d), \quad (39)$$

where P_r is the power radiated by the antenna, P_c is the power dissipated by Ohmic losses in the patch element, and P_d is the dielectric loss in the supporting substrate, given by

$$P_r = (1/4\eta)\iint \left|E_\theta E_\theta^* + E_\varphi E_\varphi^*\right| r^2 \sin\theta\, d\theta\, d\varphi, \quad (40)$$

$$P_c = Z_s \iint \left|H_\varphi^2 + H_\rho^2\right| dS, \quad (41)$$

$$P_d = (\omega \varepsilon tg\delta/2)\iint |E_z|^2\, dV. \quad (42)$$

III. NUMERICAL RESULTS AND DISCUSSION

A) Validation of results of perfect ETMA

Computer programs have been written to evaluate elements of the impedance and resistance matrices, and then solve matrix equation (30). To enhance the accuracy of the numerical calculation, the integrals of the matrix elements (31–34) are evaluated numerically along an integration path deformed above the real axis (in the complex k_s plane) to avoid the singularities. Also, Muller's method that involves three initial guesses is used for root seeking of (35). The resonant frequencies are complex and have a small positive imaginary part. The curves of Figs 3 and 4 show variation of the basis function (J_x and J_y). The number of basis functions needed to reach 3-digit accuracy in the surface-current computations was 10 functions of J_x, and 10 functions of J_y.

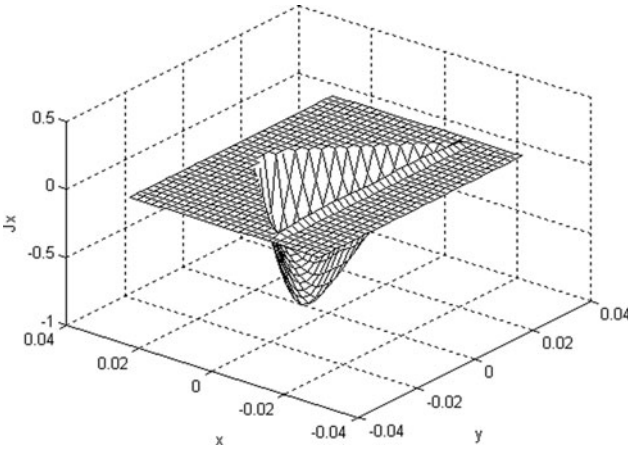

Fig. 3. Variation of the basis function J_x.

In order to validate our results, we have proceeded to a comparison with the case presented in the literature. In Fig. 5, we have calculated the resonant frequencies of TMA structure with a single layer for the mode TM_{10}, for different values of side length W and relative permittivity ε_{r2}. The considered structure was carried out by using the Galerkin method in the spectral domain. The comparison of resonant frequency was conducted for two different values of relative permittivity, which have been suggested in [12], note that the agreement is very good.

The resonant frequency of the structure presented in Fig. 1, is calculated and compared with the results presented in [13]. These results represent the effect of substrate thickness on resonant frequency, are shown in Fig. 6(a). When the substrate thickness is increased, resonant frequency increased, it is also to be noted that increasing substrate permittivity reduces resonant frequency. Very good agreement between the computation data and results of [13] is seen. The effect of substrate thickness d_2 and relative permittivity on bandwidth is shown in Fig. 6(b). It is seen that the bandwidth

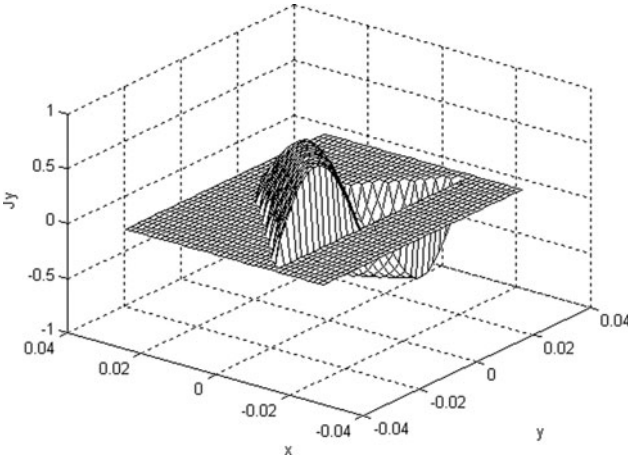

Fig. 4. Variation of the basis function J_y.

https://doi.org/10.1017/S1759078713000512 Published online by Cambridge University Press

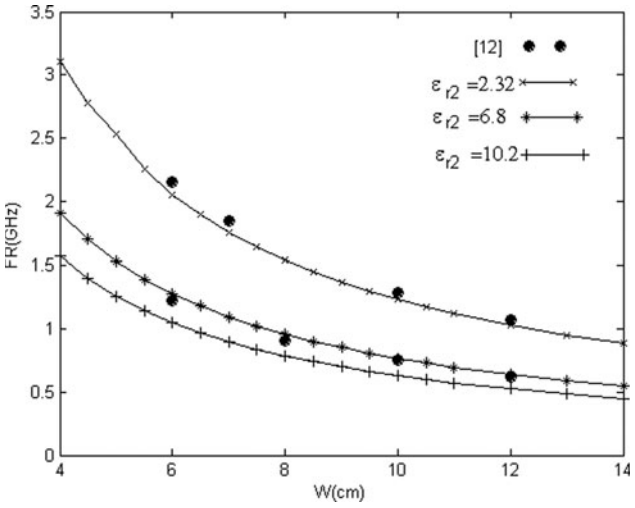

Fig. 5. Resonant frequency of a TMA against the side length $W(d_2 = 0.159$ cm, $d_1 = 0$ cm).

increases monotonically by increasing d_2 and decreases by increasing relative permittivity.

B) Resonant frequency and bandwidth of HTS equilateral triangular microstrip single layer antenna

A small microstrip antenna in high frequencies is sensitive to conductor resistance of patch because of its low radiation resistance, and decrease of radiation efficiency. In order to overcome them, the use of HTS's for the triangular patch have been proposed in this work. The influence of temperature (T) of superconducting film t of the antenna without air gap, is considered in Fig. 7. The superconducting triangular patch was assumed to be made of YBCO thin films thickness 350 nm. The superconducting material characteristics are: $\sigma_n = 10^6$ s/m, $\lambda_o = 100$ nm, and $T_c = 89$ K. It is observed that the effect of varying the temperature on resonant

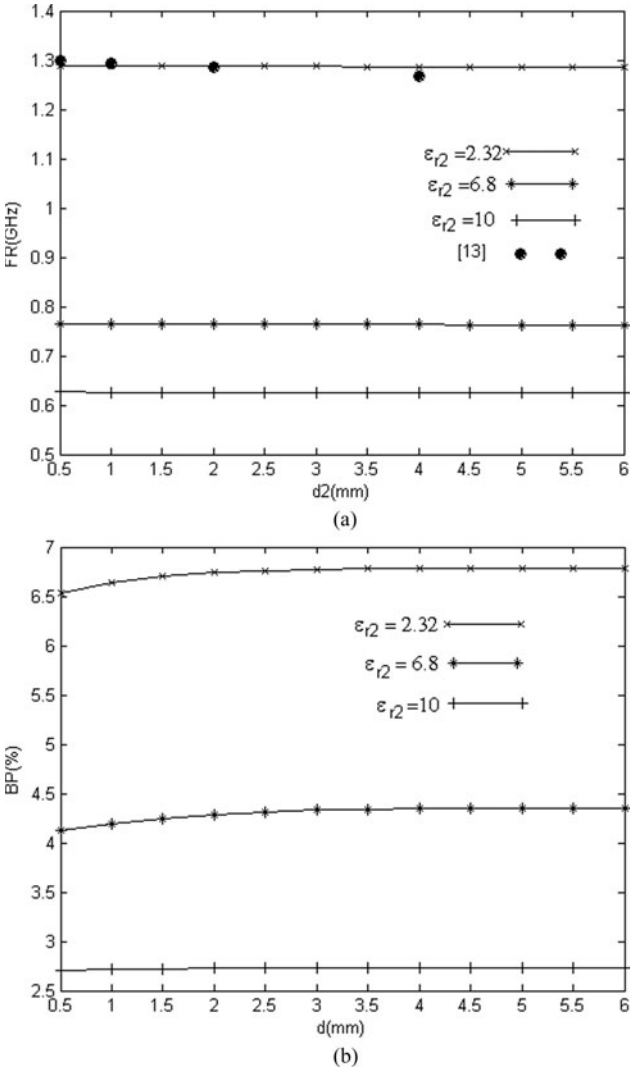

Fig. 6. (a) Resonant frequency. (b) Bandwidth versus d_2 of perfect TMA ($W =$ 10 cm, $d_1 = 0$ cm).

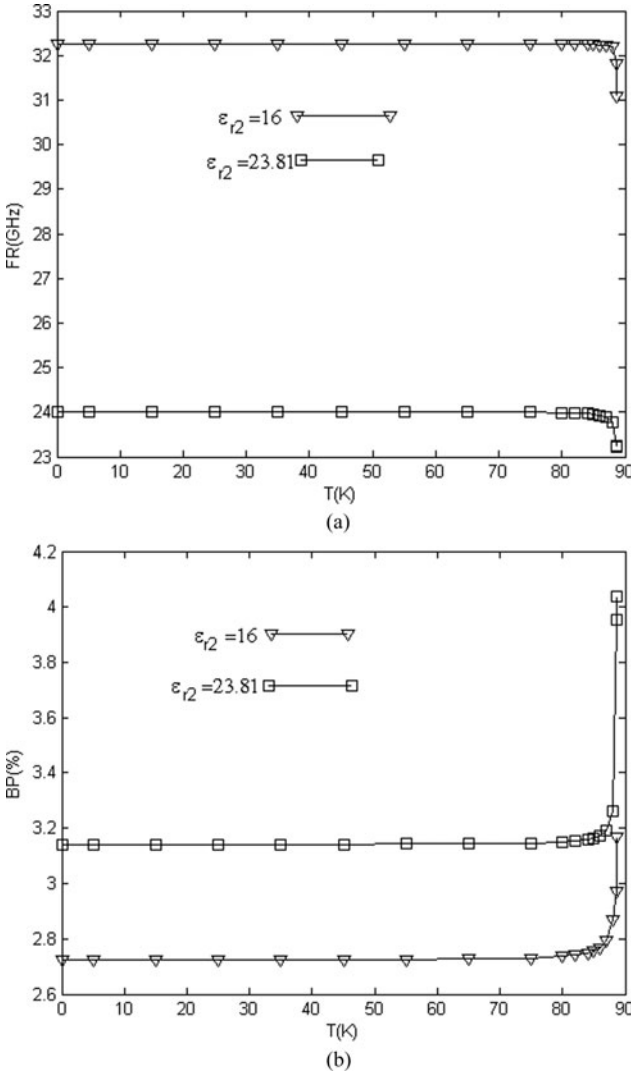

Fig. 7. (a) Resonant frequency. (b) Bandwidth versus the temperature of HTSTMA structure; $\sigma_n = 10^6$ S/m, $\lambda_o = 100$ nm and $T_c = 89$ K, $d_2 =$ 254 μm, $d_1 = 0$ mm, $t = 350$ nm, and $W = 1.4$ mm.

https://doi.org/10.1017/S1759078713000512 Published online by Cambridge University Press

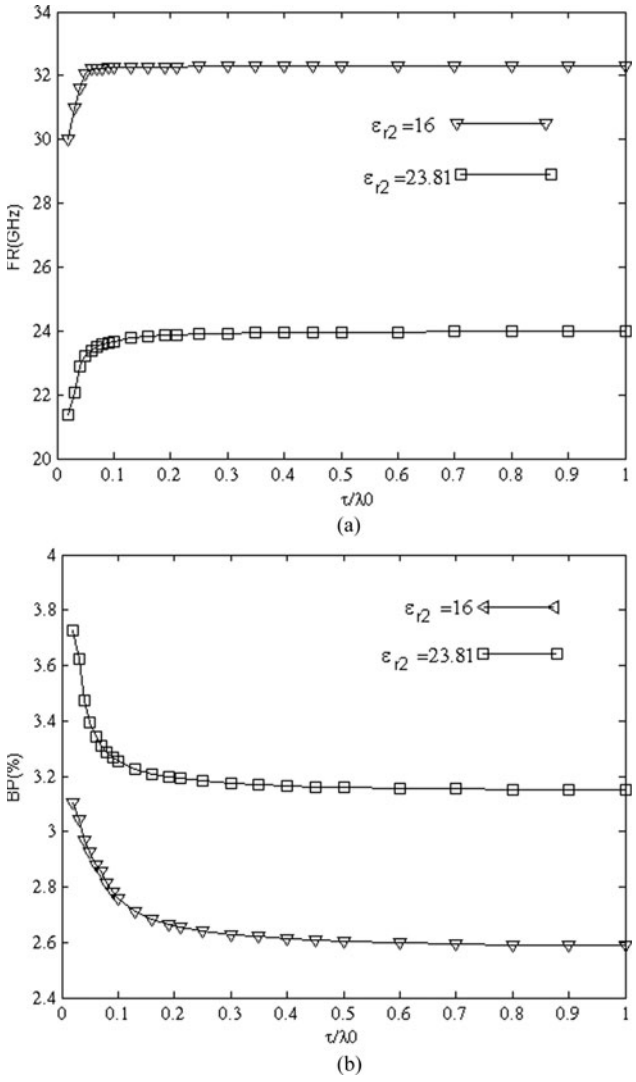

Fig. 8. (a) Resonant frequency. (b) Bandwidth versus the thickness of patch of HTSTMA structure; ($\sigma_n = 10^6$ S/m, $\lambda_o = 100$ nm and $T_c = 89$ K, $T = 50$ K, $d_2 = 254$ μm, $d_1 = 0$ mm, and $W = 1.4$ mm).

frequency and bandwidth is significant only for temperatures near the critical temperature T_c.

The dependence of resonant frequency on thickness t of superconducting patch of the antennas is shown in Fig. 8(a). It is observed that, when the film thickness t increases, the resonant frequency increases quickly until the thickness t reaches the value penetration depth λ_o. After this value, increase in the frequency of resonance becomes less significant. When t exceeds λ_o, increasing the superconducting film thickness will decrease the bandwidth slowly, as shown in Fig. 8(b).

C) Air gap tuning effect on HTS equilateral triangular microstrip

Change in the resonance frequency of a TMA with perfect conductor patch, caused by variation in air gap thickness was theoretically studied in [14, 15]. The results of these studies are compared with our theory in Table 1. The comparison among the theories and measurements shows good agreement.

Table 1. Comparison of calculated resonant frequencies of equilateral triangular microstrip patch ($W = 15.5$ mm, $d_2 = 0.508$ mm, $\varepsilon_{r2} = 2.2$, $\varepsilon_{r1} = 1$).

	Fr (GHz)			
d_1(mm)	Measured [15]	Guha [15]	Nasimuddin [14]	Present model
0.35	9.512	9.547	9.518	9.678
0.28	9.433	9.447	9.437	9.485
0.00	8.324	8.325	8.325	8.516

The tunability has been theoretically studied in Fig. 9. The design data are presented for three different substrates having widely varying dielectric constant. The superconducting patch is fabricated with a YBCO thin film. The resonant frequency normalized with respect to that with $d_1 = 0$ is plotted against (d_1/d_2) with $d_2 = 0.508$ mm. In

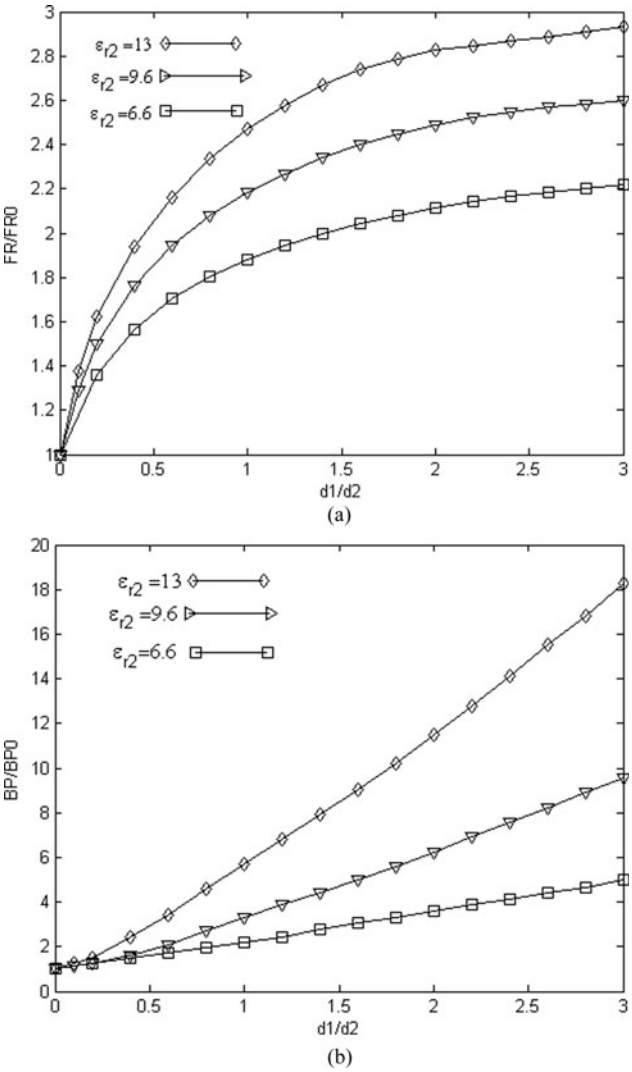

Fig. 9. (a) Resonant frequency normalized. (b) Bandwidth normalized versus d_1/d_2 of HTSTMA structure ($\sigma_n = 10^6$ S/m, $\lambda_o = 140$ nm and $T_c = 89$ K, $T = 50$ K, $d_2 = 0.508$ mm, $t = 350$ nm, and $W = 1.0$ cm). ($\varepsilon_{r2} = 13$, FRo = 5.097 GHz); ($\varepsilon_{r2} = 9.6$, FRo = 5.82 GHz); ($\varepsilon_{r2} = 6.6$, FRo = 6.87 GHz).

https://doi.org/10.1017/S1759078713000512 Published online by Cambridge University Press

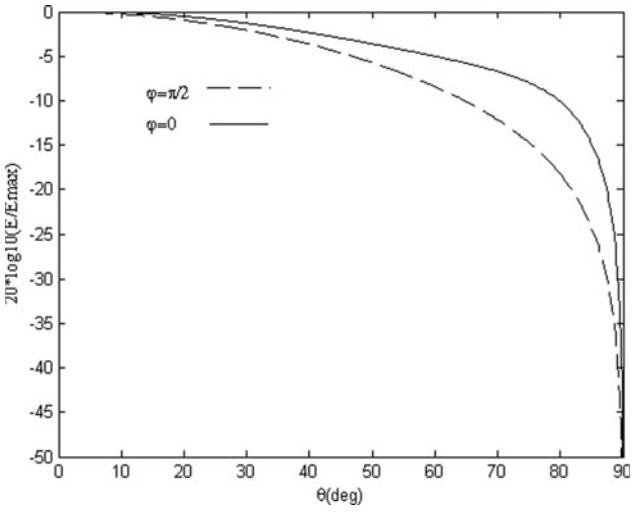

Fig. 10. Normalized radiation pattern (dB) of HTSTMA structure ($\sigma_n = 10^6$ S/m, $\lambda_o = 140$ nm and $T/T_c = 0.5$, $d_2 = 254$ μm, $t = 350$ nm, $\varepsilon_{r2} = 23.81$, and $W = 1.4$ mm). (——)E_θ ($\varphi = 0^\circ$); (– – –) E_φ ($\varphi = 90^\circ$).

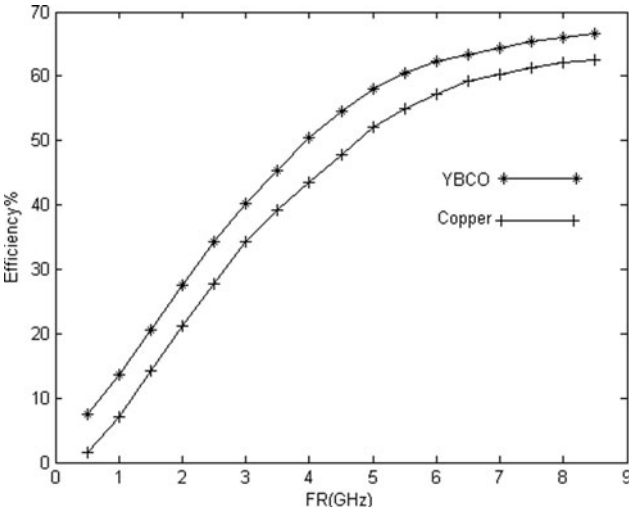

Fig. 11. HTSTMA structure efficiency ($\sigma_n = 10^6$ S/m, $\lambda_o = 140$ nm, $T/T_c = 0.5$, $\varepsilon_{r2} = 23.81$, $t_g\ \delta = 7.6\ 10^{-6}$, $d_2 = 254$ μm, $t = 350$ nm, $W = 1.4$ mm $d_1 = 0$ mm, and $\sigma_C = 40$ S/m).

Fig. 9(a), the resonant frequency versus air separation (d_1/d_2) for various substrate materials is shown. It is observed that when the air separation grows, the resonant frequency increases rapidly until achieving a maximum operating frequency at a definite air separation d_{max}. Note that the effect of the air gap is more pronounced for small values of d_1. This air gap tuning effect increases when the substrate relative permittivity value is increased. Graphical representation of the bandwidth is shown in Fig. 9(a). Note that it increases monotonically with increasing air separation.

D) Radiations patterns of HTS equilateral triangular microstrip single layer antenna

Figure 10 shows the calculated radiation patterns (electric field components, E_θ, E_φ), of the HTS equilateral triangular patch printed on substrate thickness ($d_2 = 254$ μm). The mode excited is TM_{10}. It is seen that the strongest radiation occurs in the broadside direction ($\theta = 0$).

E) Efficiency of HTSTMA structure

The efficiencies of the YBCO and copper triangular microstrip patch antennas are shown in Fig. 11. It is observed that there is a maximum improvement of 7.35% at 4.5 GHz in the efficiency of the HTSTMA structure when compared to the copper antenna at the same temperature. The benefits of using high temperature superconductors in microstrip antennas can be quite substantial owing to the reduced losses, which translates to an increase in the efficiency of the antenna [23–25].

IV. CONCLUSION

Theoretical results for resonant frequency and bandwidth have been presented for various ETMAs configurations. A spectral domain approach has been used for the numerical calculation. To include the effect of the superconductivity of the microstrip patch in spectral domain analysis, surface complex impedance has been considered. Numerical results for the effect of temperature and thickness of HTS thin film on resonant frequency and bandwidth have been presented. The properties of the HTSTMA structure were stable at temperatures slightly lower than the critical temperature. Also, computations show that the air separation can be adjusted to have the maximum operating frequency of the superconducting microstrip antenna. On the other hand, the bandwidth increases monotonically with increasing air gap width. The calculated results have been compared with the measured one available in the literature and good agreement has been found.

REFERENCES

[1] Sumantyo, J.T.S.; Ito, K.; Takahashi, M.: Dual-band circularly polarized equilateral triangular patch array antenna for mobile satellite communications. IEEE Trans. Antennas Propag., **53** (2005), 3477–3485.

[2] Helszajn, J.; James, D.S.: Planar triangular resonators with magnetic walls. IEEE Trans. Microw. Theory Tech., MTT-26 (1978), 95–100.

[3] Hansen, R.C.: Electrically Small, Superdirective, and Superconducting Antennas, John Wiley & Sons, Inc, Hoboken, New Jersey, 2006.

[4] Barkat, O.; Benghalia, A.: Radiation and resonant frequency of superconducting annular ring microstrip antenna on uniaxial anisotropic media. J. Infrared Millim. Terahertz Waves, **30** (2009), 1053–1066.

[5] Richard, M.A.; Bhasin, K.B.; Claspy, P.C.: Superconducting microstrip antennasd: an experimental comparison of two feeding methods. IEEE Trans. Antennas Propag., **41** (1993), 967–974.

[6] Cai, Z.; Bornemann, J.: Generalized spectral domain analysis for multilayered complex media and High T_c superconductor application. IEEE Trans. Microw. Theory Tech., **40** (1992), 2251–2257.

[7] Dahele, J.S.; Lee, K.F.: Theory and experiments on microstrip antennas with air gaps. Proc. Inst. Electr. Eng., H., **132** (1985), 455–460.

[8] Lee, K.F.; Luc, K.H.; Dahele, J.S.: Characteristics of the equilateral triangular patch antenna. IEEE Trans. Antennas Propag., **36** (1988), 1510–1518.

https://doi.org/10.1017/S1759078713000512 Published online by Cambridge University Press

[9] Biswas, M.; Guha, D.: Input impedance and resonance characteristics of the superstrate–loaded triangular microstrip patch. IET Microw. Antennas propag., **3** (2009), 92–98.

[10] Hassani, H.R.; Syahkal, D.M.: Analysis of triangular patch antennas including radome effects. IEE Proc., **139** (1992), 251–256.

[11] Staraj, R.; Cambiaggio, E., Papiernik, A.: Infinite phased arrays of microstrip antennas with parasitic elements: application to bandwidth enhancement. IEEE Antennas Propag., **42** (1994), 742–746.

[12] Nachit, A.; Foshi, J.: Spectral domain integral equation approach of an equilateral triangular microstrip antenna using the moment method. Journal of Microwaves and Optoelectronics., **2** (2000), 1–13.

[13] Chen, W.; Lee, K.F.; Dahele, S.: Theoretical and experimental studies of the resonant frequencies of the equilateral triangular microstrip antenna. IEEE. Antennas Propag., **40** (1992), 1253–1256.

[14] Nasimuddin.; Esselle, K.; Verma, A.K.: Resonance frequency of an equilateral triangular microstrip antenna. Microw. Opt. Technol. Lett., **47** (2005), 485–489.

[15] Guha, D.; Siddiqui, J.Y.: Resonance frequency of equilateral triangular microstrip antenna with and without air gap. IEEE Trans. Antennas Propag., **52** (2004), 2174–2177.

[16] Dreher, A.: A new approach to dyadic Green's function in spectral domain. IEEE Trans. Antennas Propag., **43** (1995), 1297–1302.

[17] Das, N.K.; Pozar, D.M.: A generalized spectral-domain Green's function for multilayer dielectric substrates with application to multilayer transmission lines. IEEE Trans. Microw. Theory Tech., MTT-35 (1987), 326–335.

[18] Bouttout, F.; Benabdelaziz, F., Fortaki, T.; Khedrouche, D.: Resonant frequency and bandwidth of a superstrateloaded rectangular patch on a uniaxial anisotropic substrate. Commun. Numer. Methods Eng., **16** (2000), 459–473.

[19] Chew, W.C.; Liu, Q.: Resonance frequency of a rectangular microstrip patch. IEEE Trans. Antennas Propag., **36** (1988), 1045–1056.

[20] Gorter, J.C.; Casimir, H.B.G.: The Thermodynamics of the superconducting state. Phys. Z., **35** (1934), 963–966.

[21] Porch, A.; Lancaster, M.J.; Humphreys, R.G.: The coplanar resonator technique for determining the surface impedance of YBa2Cu3O7-d thin film. IEEE Trans. Microw. Theory Tech., **43** (1995), 306–314.

[22] Cho, S.: Inductance measurements in YBa2Cu3O7-x thin films. Supercond. Sci. Tech., **10** (1997), 594–597.

[23] Silva, S.G.; D'assuncao, A.G.: Oliveira, J.R.S.: Analysis of high T_c superconducting microstrip antennas and arrays. Proc. SBMO/IEEE MTT-SIMOC, **2** (1999), 243–246.

[24] Sekiya, N.; Kubota, A.; Kondo, A.; Hirano, S.; Saito, A.; Ohshima, S.: Broadband superconducting microstrip patch antenna using additional gap-coupled resonators. Physica C., **445–448** (2006), 994–997.

[25] EL-Ghazaly, S.M.; Hammond, R.B.; Itoh, T.: Analysis of superconducting microwave structures: application to microstrip lines. Trans. Microw. Theory Tech., **40** (1992), 499–508.

O. Barkat was born in Constantine, Algeria in 1974. She received her Engineering Diploma in electronic engineering in 1999, as a Master in microwaves in 2002 and Ph.D. degrees in microwaves in 2009 from the Electronic Institute, University of Constantine. Currently, she is working as a Professor in the Department of Electronics Engineering. Her main field of interest is millimeter-wave antennas, active and passive circuits, antenna arrays, EBG structures, and their applications for microwave devices.

https://doi.org/10.1017/S1759078713000512 Published online by Cambridge University Press